Received: 11 September 2019 | Revised: 21 January 2020 | Accepted: 5 February 2020

DOI: 10.1002/ces2.10038

International Journal of Ceramic Engineering & Science

ORIGINAL ARTICLE

Spark plasma sintering of alumina/yttria-doped silicon carbide

Antonio Popolizio | **Mattia Biesuz** | **Alberto Molinari** | **Vincenzo M. Sglavo**

Department of Industrial Engineering, University of Trento, Trento, Italy

Correspondence
Mattia Biesuz, Department of Industrial Engineering, University of Trento, Via Sommarive 9, 38123 Trento, Italy.
Email: mattia.biesuz@unitn.it

Abstract

Silicon carbide possesses exceptional mechanical and thermal properties, but its densification by conventional sintering is often very difficult. In the present work, silicon carbide was consolidated by spark plasma sintering in the presence of alumina and yttria. The results pointed out that the use of a single oxide does not enhance the sintering kinetics significantly, while the contemporaneous addition of both oxides has a beneficial effect on densification, with a relative density increase of about 10%. Interestingly, the oxide doping allows to double the room-temperature flexural strength.

KEYWORDS

field-assisted sintering technology, liquid-phase sintering, silicon carbide, sinter/sintering, spark plasma sintering

1 | INTRODUCTION

Silicon carbide (SiC) is a covalent ceramic characterized by unique combination of physical and mechanical properties (ie, low density, high hardness,[1] high elastic modulus,[2] low nuclear activation,[3] low thermal expansion coefficient, high-temperature strength[4]), which make it an optimum candidate for very different applications.[1,2] Unfortunately, its sinterability is relatively limited and the consolidation of SiC-based components usually requires sophisticated and expensive technologies such as hot pressing (HP)[5] or hot isostatic pressing (HIP).[6]

Over the years, alternative sintering techniques have been developed with the aim to reduce dwell time and temperature such as field-assisted sintering techniques (FAST) and, in particular, spark plasma sintering (SPS).[7–9]

Spark plasma sintering consists of a mechanical loading system such as HP, but instead of an external heating, a pulsed electric current flows through the punches, through the mold, and, depending on the electrical conductivity, also through the powder compact within the die.[10] Thanks to the good electrical conductivity of the materials used for the mold (typically, graphite), low voltages (in general, below 10 V) generate high currents (from about 1 to 10 kA), leading to efficient Joule heating. Even in the case of electrically non-conductive sintering powder, such as SiC, heat is quickly and efficiently transferred to the sample. SPS allows to increase the heating rates with respect to HP and, consequently, allows a reduction of the processing time.[7–9] The current flow can significantly improve the mass transfer also by other athermal mechanisms involving diffuse electrical field, thermo-diffusion,[11] electromigration,[12,13] and/or spark plasma formation,[14] the formation of plasma being still under debate.[15,16] High heating rates, short processing times, and low temperatures are possible with SPS, and this allows the production of highly densified materials with good control of grain coarsening. SiC densification by SPS has been extensively studied to point out the impact of processing parameters, such as pressure, holding time, and temperature, on densification.[17,18]

The formation of a liquid phase upon sintering allows improved densification by particle rearrangement and dissolution/reprecipitation mechanisms.[19,20] The addition of dopants to

increase the sinterability of SiC has been largely studied during the last decades. Some activities have been focused on the use of oxides,[21–25] which enhance the final densities by the activation of liquid-phase sintering (LPS).[21,23] The most popular addictives were SiO_2, Al_2O_3, and Y_2O_3.[21–25] SiO_2 was in particular proved to be very effective, but it has a deleterious effect on the high-temperature strength (leaving a grain boundary glassy phase). Moreover, it causes undesired high-temperature reaction ($SiO_2 + SiC \rightarrow SiO_{(g)} + CO_{(g)}$), thus limiting the sintering temperature window (well below 1900°C even in CO atmosphere).[22] Other researches were focused on the use of refractory oxynitride compounds[26,27] or boron[28] as LPS promoters. Finally, carbon-based materials (including multilayer graphene, carbon black, pyrolytic graphite, graphite) were used as sintering aids for SiC[29–31] as they reduce the kinetics of non-densifying coarsening mechanisms, including surface diffusion and evaporation/condensation.[31]

Despite the existing literature on SiC sintering in the presence of Y_2O_3 and Al_2O_3, a comprehensive analysis comparing the effect of the single oxide addition and of their mixture is still missing. The goal of the present research work was to study SiC densification upon SPS with the addition of Y_2O_3 and Al_2O_3 (or their mixture) used as potential sintering promoters. The effect is analyzed on two different SiC powders with different grain size distribution.

2 | EXPERIMENTAL PROCEDURE

Two different silicon carbide powders were employed in this work: SiC ABR I F1500 S (Sika®) and SiC FCP 15 NLC RTP (Norton AS). The first one (identified as coarse powder) is characterized by sharp-shaped particles with mean diameter of about 2 μm; the other one (named as fine powder) is constituted by isometric particles with diameter in 0.1-1 μm range.

To improve the silicon carbide powder densification upon SPS, alumina and yttria were used as sintering aids. The oxides were obtained by thermal decomposition of the corresponding nitrates, aluminum nitrate nonahydrate $Al(NO_3)_3.9H_2O$ (Ensure®) and yttrium (III) nitrate hexahydrate $Y(NO_3)_3.6H_2O$ (Sigma-Aldrich®). Thermogravimetric analysis (TGA) and differential thermal analysis (DTA) were preliminarily carried out on the two nitrates to identify their decomposition temperature. The analyses were carried out up to 1200°C with heating rate of 10°C/min using a Netzsch STA409 thermobalance operating in air atmosphere. The calcination cycle was then performed at 700°C (heating rate = 5°C/min) with 1-hour duration. Further, TGA and DTA experiments were carried out on calcined powder in order to verify their thermal behavior.

Variable amount of oxides was added to SiC powders, as detailed in Table 1. The specified nitrate amount was dissolved in ethanol (96° by Sigma-Aldrich®) and manually mixed with SiC powder. The obtained slurry was initially heated at 90°C for the complete ethanol evaporation; then, it was calcined in a muffle at 700°C for 1 hour under static air (heating rate = 10°C/min).

The obtained powder mixtures were used for the spark plasma sintering in a graphite die (diameter = 10 mm for SPS1 cycle, 20 mm for SPS2-5 cycles) using Dr SINTER SPS1050 machine. The internal cavity of the die was covered by a graphite foil in order to allow the electrical current flow. The weight of each sample was about 5 g. The sample temperature was monitored during the SPS cycle using a pyrometer pointing on the graphite die at about 4 mm from the specimen (acquisition frequency = 1 Hz). All the parameters used for SPS are summarized in Table 2.

Once the samples were sintered, their thickness and diameter were measured by a digital caliper (sensitivity ± 0.01 mm). These values, combined with the piston displacement recorded by the SPS machine, were used to estimate the sample deformation upon sintering.

The density was evaluated by the Archimedes' method (ASTM C830) using an analytical balance (Gilbertini, sensitivity ± 0.1 mg). SEM micrographs were taken using JOEL IT300 and JOEL JSM-550 microscopes on the fracture surface of the sintered specimens to evaluate their microstructure; the specimens were coated with Pt/Pd alloy (QUORUMQ 150T coater) by sputtering in advance. The phase composition analysis was carried out on the sintered samples by XRD, using RIGAKU D-MAX III diffractometer with a graphite microchromator ($2\theta = 25°$-$50°$, X-ray source: Cu-Kα, 0.154184 nm). Mechanical tests were also performed in order to evaluate the flexural strength by piston-on-three-balls configuration using MTS 810 servo-hydraulic machine (MTS®).

3 | CALCULATIONS

In order to analyze the densification behavior of SiC upon SPS, the relative density evolution was estimated using the SPS cross-bar displacement data (recorded by the machine), the mass, the final thickness, and diameter of the sintered specimens. One should consider that the cross-bar displacement includes two different effects, the sintering shrinkage and the thermal strain. Therefore, it is necessary to distinguish

TABLE 1 Composition of the batches used in the present work

Powder mixture	SiC [wt%]	Al_2O_3 [wt%]	Y_2O_3 [wt%]
Pure SiC	100	—	—
5A	95	5	—
5Y	95	—	5
2.5AY	95	2.5	2.5
5AY	90	5	5

TABLE 2 SPS cycles used on different powder mixtures (free cooling in vacuum)

SPS cycle	Powder mixture	Maximum temperature [°C]	Pressure [MPa]	Temperature of pressure application [°C]	Heating rate [°C/min]	Holding time T_{max} [min]
SPS1	Pure SiC	2300	60	1200	200	3
SPS2	Pure SiC	1900	0	—	100	3
	2.5AY	1900	0	—	100	3
SPS3	Pure SiC	1900	60	1200	100	3
	2.5AY	1900	60	1200	100	3
	5AY	1900	60	1200	100	3
SPS4[a]	Pure SiC	1800	60	1200	100	5
	5A	1800	60	1200	100	5
	5Y	1800	60	1200	100	5
SPS5	2.5AY	1900	60	700	100	3

[a]The cycle SPS4 was used only in the case of coarse powder.

the two contributions to evaluate the density variation as a function of temperature.

The thermal expansion was approximated by a second-order polynomial function, estimated in the low-temperature range before any sintering shrinkage occurs. Therefore, under the assumption that the thermal expansion follows the same trend also at higher temperature, it is possible to determine the thermal expansion contribution to the total displacement.

The displacement associated with sintering is therefore calculated by subtracting the thermal expansion displacement from the total displacement recorded by the SPS machine.

Once the real shrinkage is calculated, it can be used to determine the instantaneous relative density upon sintering. The initial thickness of the powder compact (h_0) is unknown but can be calculated as the sum of the final thickness of sintered sample (h_{fin}) and the maximum displacement (Δh_{max}) due to the sintering shrinkage:

$$h_0 = h_{fin} + \Delta h_{max} \tag{1}$$

The hypothesis is made here that the elastic recovery after the removal of the pressure is negligible with respect to Δh_{max}. The sample thickness at a given temperature ($h_{(T)}$) is determined as the sum of the initial one and the net displacement calculated at the same temperature ($\Delta h_{(T)}$):

$$h_{(T)} = h_0 + \Delta h_{(T)} \tag{2}$$

The sample volume ($V_{(T)}$) is easily determined as:

$$V_{(T)} = h_{(T)} \pi r^2 \tag{3}$$

where r is the internal radius of the die (r = 10 mm). Also in this case, possible elastic deformations of the die are considered very small and therefore neglected.

Starting from the instantaneous volume of powders, one can calculate the density ($\rho_{(T)}$) and the relative density ($RD_{(T)}$) for each powder mixture during the entire sintering cycle as:

$$\rho_{(T)} = \frac{m}{V_{(T)}} \tag{4}$$

$$RD_{(T)} = \frac{\rho_{(T)}}{\rho_{th}} \tag{5}$$

where ρ_{th} is the theoretical density of the mixture calculated starting from the theoretical density of each compound by the rule of mixtures. The derivative of $RD_{(T)}$ is considered in this work to point out the different phenomena leading to densification.

4 | RESULTS AND DISCUSSION

Sintering cycle SPS1 can be considered as a conventional high-temperature SPS cycle for SiC; the specimens were heated up to 2300°C, and 60 MPa pressure was applied starting from 1200°C. Figure 1 shows the consolidation behavior of pure, fine and coarse, SiC powders upon SPS1 cycle. These curves can be assumed as reference for the other cycles studied in the present work. The behavior of fine and coarse SiC powder is shown by the derivative of the RD calculated from Equation 5. One can observe a peak at about 1200°C for both materials, which is associated with the rearrangement of the powder determined by the pressure application. The densification starts at about 1800°C.

The coarse powder shows a double shrinkage (at ~1800°C and ~2000°C), which can be probably related to different sintering mechanisms. This can be likely associated with: (a)

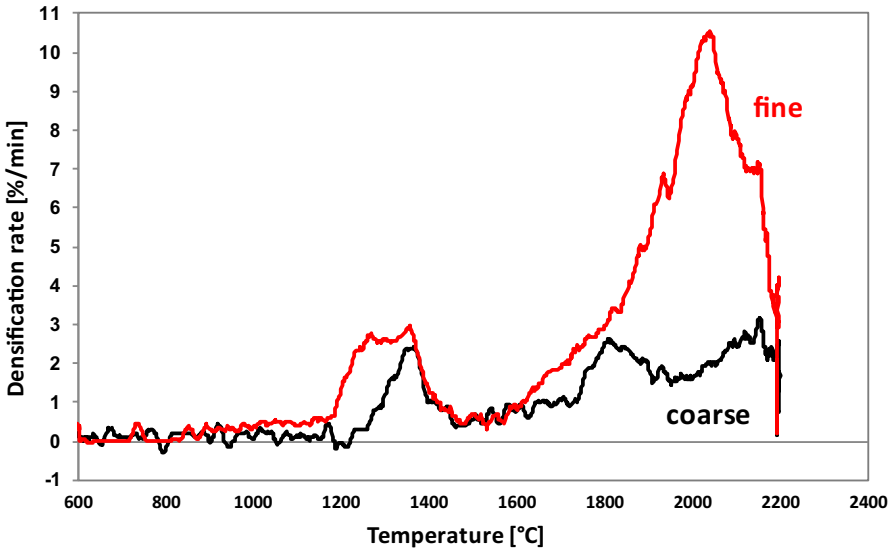

FIGURE 1 Densification rate curve for pure SiC powders (coarse and fine) during SPS1 cycle

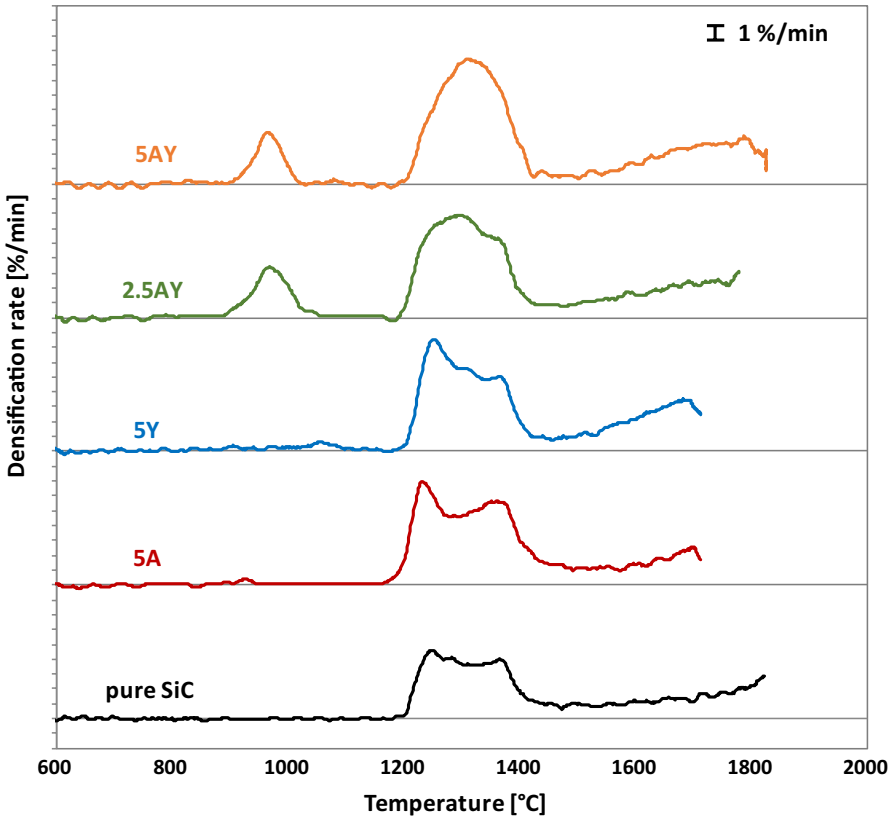

FIGURE 2 Densification rate for coarse powder–containing mixtures during SPS3 and SPS4 cycle

the presence in the sample of powders with different size; or (b) an initial rounding of the sharp particle edges (~1800°C) followed by neck growth and sintering (~2000°C).

Conversely, in the case of fine and isometric-equiaxial powder, only one intense peak is registered starting from 1800°C. The strong densification of fine powder is numerically confirmed by the final relative density equal to 95%, much higher than in coarse powder sample (68%).

The effect of sintering aids on the densification rate is shown in Figures 2 and 3. One can point out that the densification rate of alumina- or yttria-doped SiC (Figure 3) is very similar to pure SiC. Tables 3 and 4 summarize the relative density data measured experimentally and estimated from the SPS cross-bar data; flexural strength results are also reported. Interestingly, data calculated from the SPS densification curves match very well with the experimental measurements; such data also point out that Al_2O_3 or Y_2O_3 addition slightly improves the final density by only ~4% (from ~56% in the undoped powder to ~60% for the doped ones; Table 3). The flexural strength does not show any improvement, too.

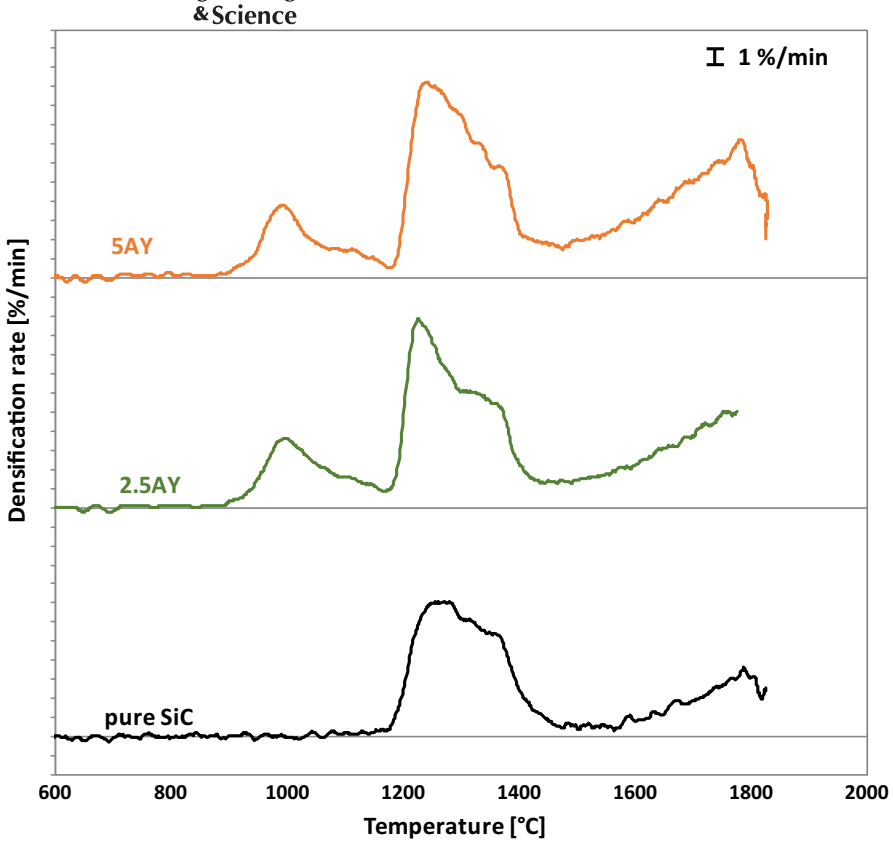

FIGURE 3 Densification rate for fine powder–containing mixtures during SPS3 cycle

Therefore, the addition of one single oxide is not efficient for enhancing SiC densification.

Conversely, a significant densification enhancement is achieved by adding both oxides together (2.5AY and 5AY samples): 2.5AY samples are characterized by a relative density generally 10% higher than pure SiC, the improvement being higher (about 20%) in the case of 5AY composition. The improved densification has a reflex also on the mechanical properties, the strength being often doubled (or more) than in pure SiC samples. The enhanced mechanical properties can be primarily attributed to the improved densification in the presence of Al_2O_3/Y_2O_3. The differences are strongly reduced if one compares samples with similar densities but with or without Al_2O_3/Y_2O_3 addition (ie, sample 2.5AY treated by SPS2 and pure SiC treated by SPS3, in case of both coarse and fine powders). It is also important to point out that Al_2O_3/Y_2O_3 addition allows to reduce the maximum sintering temperature by about 400°C.

The shrinkage rate reveals a relatively complex sintering behavior for 2.5AY and 5AY mixtures with respect to the others (Figures 2 and 3). In particular, one can observe the presence of a low-temperature (at about 950°C) shrinkage phenomenon, which is absent in 5A and 5Y samples. It is worth pointing out that such event does not require

TABLE 3 Relative densities and flexural strength for samples produced from coarse SiC powder

SPS cycles	Powder mixtures	RD by Archimedes' method [%]	RD by SPS data [%]	Flexural strength [MPa]
SPS1	Pure SiC	68	70	—
SPS2	Pure SiC	48	48	43-52
	2.5AY	60	60	112-127
SPS3	Pure SiC	59	59	130-151
	2.5AY	66	67	197-212
	5AY	71	71	220-259
SPS4	Pure SiC	56	56	58-103
	5A	60	58	42-62
	5Y	60	60	52-54
SPS5	2.5AY	67	68	206-243

TABLE 4 Values of relative densities and flexural strength for samples produced from fine SiC powder

SPS cycles	Powder mixtures	RD by Archimedes' method [%]	RD by calculation on SPS data	Flexural strength [MPa]
SPS1	Pure SiC	95	99	—
SPS2	Pure SiC	53	52	33-35
	2.5AY	66	65	142-196
SPS3	Pure SiC	67	67	87-147
	2.5AY	79	77	291-356
	5AY	87	85	372-376
SPS5	2.5AY	78	78	331-393

any external pressure to take place, it being observed well before the load application temperature (1200°C). The origin of such initial shrinkage phenomenon is not completely clear. Two different effects can be considered. First, one can propose that Al_2O_3 and Y_2O_3 react with SiO_2 present on SiC particles surface and very likely formed during the calcination stage. The three oxides could form a glassy phase whose softening is responsible for particle rearrangement and shrinkage. Such hypothesis is consistent with some literature data on Al_2O_3-Y_2O_3-SiO_2 glasses whose glass transition temperature (T_g) was reported to be even lower than 950°C.[32] Alternatively, one can suggest that some transformations take place on the Al_2O_3/Y_2O_3-doped powder causing a molar volume variation and a rearrangement of the green body structure. To verify this hypothesis, DTA was carried out using different heating rates on the two oxide mixture prepared following the same procedure previously described (dissolution in ethanol of the nitrates, drying, and calcinations at 700°C). The thermal analyses, reported in Figure 4, point out the presence of an exothermic peak between ~930°C and 970°C, slightly variable with the heating rate (in the range 2-40°C/min). To identify the position at the heating rate used in SPS cycle (100°C/min), the peak position displacement was modeled by the relationship:[33–35]

$$\frac{T_p^2}{HR} = e^{\frac{Q}{R}\frac{1}{T_p}} \quad (6)$$

where T_p is the temperature of the peak; HR, the heating rate; Q, the activation energy; and R, the universal gas constant.

The fit of the experimental data (Figure 4) by Equation 6 allows to estimate an activation energy for the phase transition of 934 kJ/mol. The peak temperature corresponding to heating rate of 100°C/min (the heating rate used for all the SPS cycles) is 985°C. Therefore, the densification peak in Figures 2 and 3 well matches the exothermic peak associated with the reaction of two oxides at 100°C/min.

In order to identify the nature of this exothermic event, XRD analysis was carried out on the two oxide mixture before and after the exothermic peak. The patterns reported in Figure 5 show that after calcination at 700°C, the alumina/yttria mixture is still amorphous, whereas at higher temperature, yttrium aluminum garnet (YAG, $Y_3Al_5O_{12}$) crystallizes.

The microstructure of the sintered samples was characterized by XRD, SEM, and EDS in order to verify the previous hypotheses. Figure 6 shows the XRD spectra recorded on the 5YA sintered specimens. Two main phases

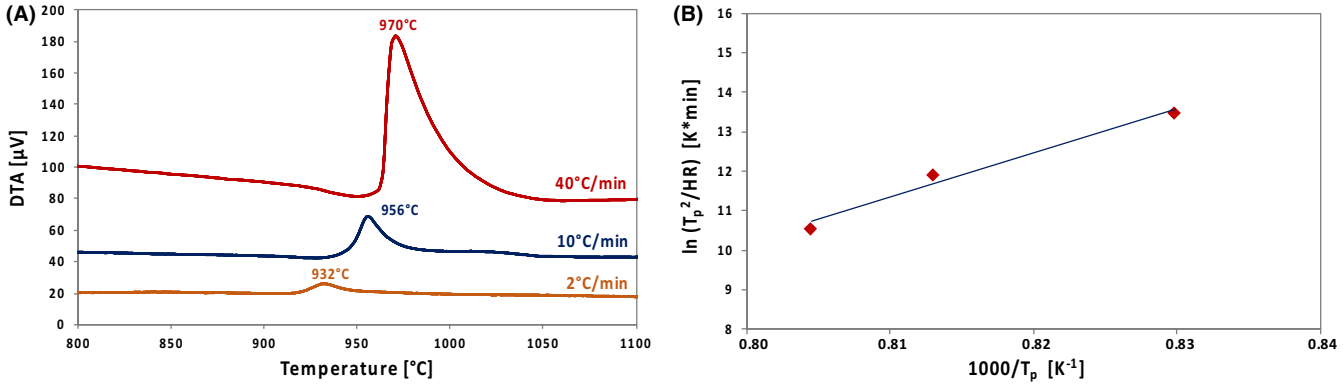

FIGURE 4 DTA on calcined salts (Al_2O_3-Y_2O_3) with different heating rates (A); fitting of the experimental points for the determination of YAG crystallization activation energy (B)

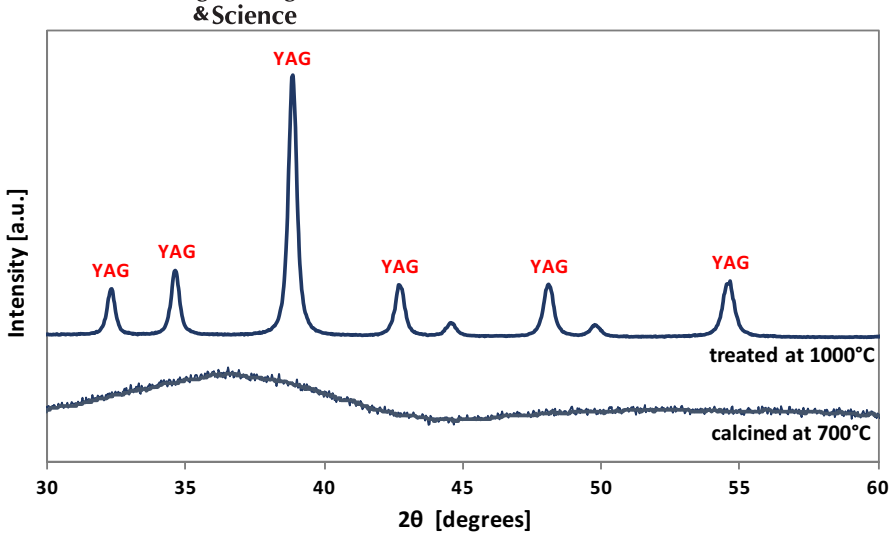

FIGURE 5 XRD spectrum of alumina/yttria mixture after thermal treatment at 700 and 1000°C

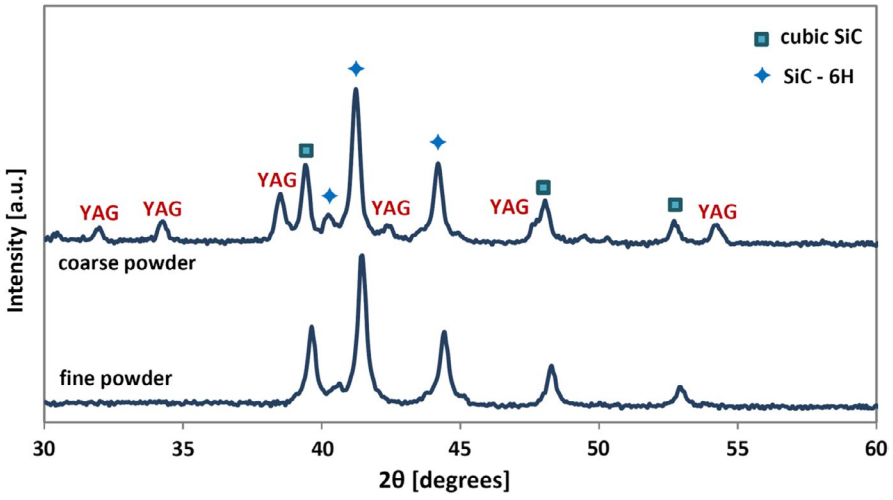

FIGURE 6 XRD spectrum of samples obtained by sintering powder (fine and coarse) mixture 5AY

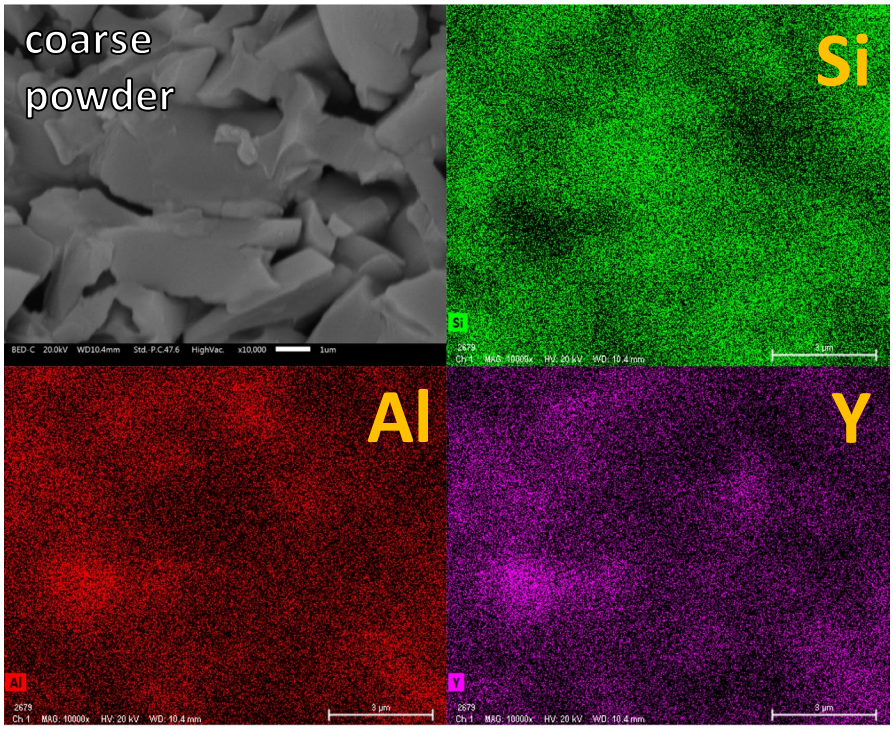

FIGURE 7 Elemental mapping by EDXS analysis on fracture surface of SiC sintered (SPS3) component obtained by 5AY mixture with coarse SiC powder

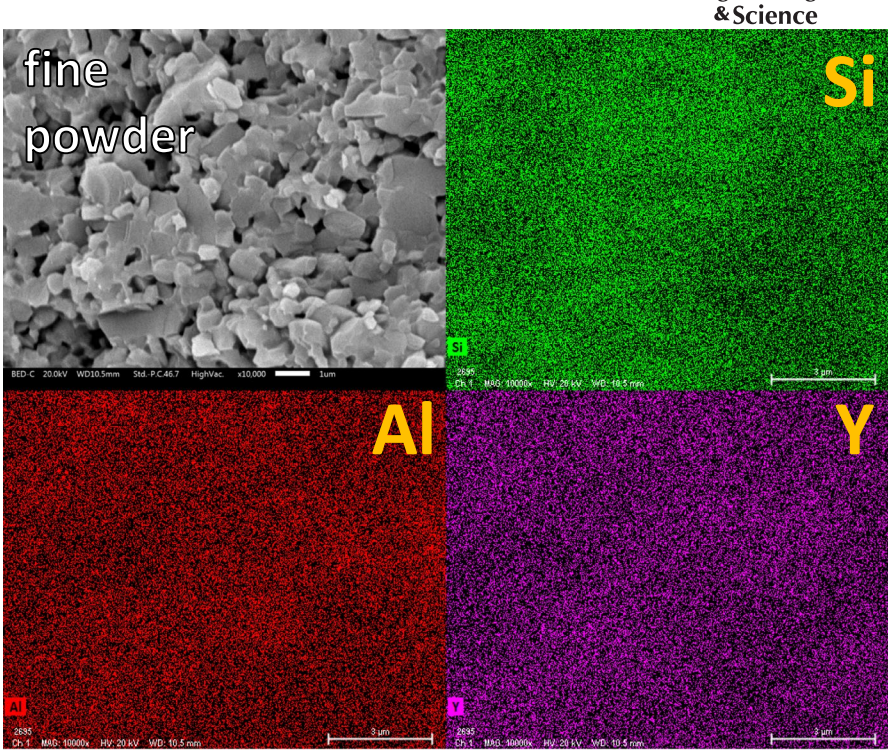

FIGURE 8 Elemental mapping by EDXS analysis on fracture surface of SiC sintered (SPS3) component obtained by 5AY mixture with fine SiC powder

are revealed when fine powder is used the most abundant being moissanite (SiC, hexagonal structure) with limited amount of cubic SiC. Conversely, a third phase appears when coarse powder mixture is used, corresponding to yttrium aluminum garnet. EDS elemental mapping results, shown in Figure 7, confirm the presence of Y-Al–localized concentration in the samples (coarse powder). One can easily observe that yttrium and aluminum are localized in the same regions, which in turn are poorer in silicon (this excludes an experimental origin for said Y and Al concentration fluctuations). Conversely, a homogeneous presence of Al and Y is revealed (Figure 8) in the specimen produced starting from SiC fine powder. It is worth to point out that the use of equivalent alumina/yttria mass as sintering aid (Table 1) does not correspond exactly to the stoichiometric composition of YAG, a certain amount (around 30%) of Y_2O_3 remaining in excess and probably being solubilized by silica present on SiC particle surface. The origin of the difference in the materials produced using the two powders can be related to the higher reactivity of the fine powder, which was probably oxidized more during the calcination process. As a matter of fact, the formation of a larger amount of SiO_2 could have led to the formation of a liquid/glassy phase among silica, alumina, and yttria, thus inhibiting the crystallization of the garnet (YAG).

5 | CONCLUSIONS

This work is focused on investigating the effect of alumina and yttria as sintering aids on spark plasma sintering of SiC. The concomitant addition of alumina and yttria on two different powders leads to higher final relative density and mechanical properties, whereas no relevant improvements are obtained by the addition of alumina and yttria alone.

Finally, one could state that the yttria-alumina combined presence can anticipate the densification temperature of SiC by about 400 K. The effect is very likely related to the softening of a glassy phase or the volumetric shrinkage upon YAG formation and to more efficient diffusion mechanisms.

ACKNOWLEDGMENTS

The authors kindly acknowledge the support from the Italian Ministryof University and Research (MIUR) within the programs PRIN2017 -2017FCFYHK "DIRECTBIOPOWER", PRIN2017 - 2017PMR932"Nanostructured Porous Ceramics for Environmental and Energy Applications" and Departments of Excellence 2018-2022 (DIIUNITN).

ORCID

Mattia Biesuz https://orcid.org/0000-0002-4338-4177
Vincenzo M. Sglavo https://orcid.org/0000-0001-9133-7204

REFERENCES

1. Kimoto T, Cooper JA. Fundamentals of silicon carbide technology. New York, NY: Wiley, 2014.
2. Vargas-Gonzalez L, Speyer RF, Campbell J. Flexural strength, fracture toughness, and hardness of silicon carbide and boron carbide armor ceramics. Int J Appl Ceram Technol. 2010;7: 643–51.

3. Price RJ. Properties of silicon carbide for nuclear fuel particle coatings. Nucl Technol. 1977;35:320–36.
4. Keppeler M, Reichert H, Broadley JM, Thurn G, Wiedmann I, Aldinger F. High temperature mechanical behaviour of liquid phase sintered silicon carbide. J Eur Ceram Soc. 1998;18:521–6.
5. Sajgalík P, Sedlácek J, Lences Z, Dusza J, Lin HT. Additive-free hot-pressed silicon carbide ceramics—a material with exceptional mechanical properties. J Eur Ceram Soc. 2016;36:1333–41.
6. Jihong S, Jingkun G, Dongliang J. Hot isostatic pressing of alpha-silicon carbide ceramics. Ceram Int. 1993;19:347–51.
7. Orrù R, Licheri R, Locci AM, Cincotti A, Cao G. Consolidation/synthesis of materials by electric current activated/assisted sintering. Mater Sci Eng R. 2009;63:127–287.
8. Grasso S, Sakka Y, Maizza G. Electric current activated/assisted sintering (ECAS): a review of patents 1906–2008. Sci Technol Adv Mater. 2009;10:053001.
9. Guillon O, Gonzalez-Julian J, Dargatz B, Kessel T, Schierning G, Räthel J, et al. Field-assisted sintering technology/spark plasma sintering: Mechanisms, materials, and technology developments. Adv Eng Mater. 2014;16:830–49.
10. Manière C, Lee G, Olevsky EA. All-materials-inclusive flash spark plasma sintering. Sci Rep. 2017;7:15071.
11. Olevsky EA, Froyen L. Impact of thermal diffusion on densification during SPS. J Am Ceram Soc. 2009;92:122–32.
12. Olevsky EA, Dudina DV. Field-assisted sintering. Cham, Switzerland: Springer, 2018.
13. Frei JM, Anselmi-Tamburini U, Munir ZA. Current effects on neck growth in the sintering of copper spheres to copper plates by the pulsed electric current method. J Appl Phys. 2007;101:114914.
14. Chaim R. Densification mechanisms in spark plasma sintering of nanocrystalline ceramics. Mater Sci Eng A. 2007;443:25–32.
15. Hulbert DM, Anders A, Andersson J, Lavernia EJ, Mukherjee AK. A discussion on the absence of plasma in spark plasma sintering. Scr Mater. 2009;60:835–8.
16. Saunders T, Grasso S, Reece MJ. Plasma formation during electric discharge (50V) through conductive powder compacts. J Eur Ceram Soc. 2014;35:871–7.
17. Guillard F, Allemand A, Lulewicz J, Galy J. Densification of SiC by SPS-effects of time, temperature and pressure. J Electrochem Soc. 2007;27:2725–8.
18. Hayun S, Paris V, Mitrani R, Kalabukhov S, Dariel MP, Zaretsky E, et al. Microstructure and mechanical properties of silicon carbide processed by Spark Plasma Sintering (SPS). Ceram Int. 2012;38:6335–40.
19. German RM. Liquid phase sintering, vol. 39. New York, NY: Springer Science, 1985.
20. Rahaman MN. Ceramic processing and sintering. New York, NY: Marcel Dekker, 1996.
21. Gomez E, Echeberria J, Iturriza I, Castro F. Liquid phase sintering of SiC with additions of Y_2O_3, Al_2O_3 and SiO_2. J Eur Ceram Soc. 2004;24:2895–903.
22. Ye H, Rixecker G, Aldinger F. Liquid phase sintered SiC with SiO_2 additive. Ceram Process Reliab Tribol Wear. 2000;12:172–7.
23. van Dijen FK, Mayer E. Liquid phase sintering of silicon carbide. J Eur Ceram Soc. 1996;2219:413–20.
24. Gubernat A, Stobierski L, Łabaj P. Microstructure and mechanical properties of silicon carbide pressureless sintered with oxide additives. J Eur Ceram Soc. 2007;27:781–9.
25. She JH, Ueno K. Effect of additive content on liquid-phase sintering on silicon carbide ceramics. Mater Res Bull. 1999;34:1629–36.
26. Nader M, Aldinger F, Hoffmann MJ. Influence of the α/β -SiC phase transformation on microstructural development and mechanical properties of liquid phase sintered silicon carbide. J Mater Sci. 1999;34:1197–204.
27. Schneider J, Biswas K, Rixecker G, Aldinger F. Microstructural changes in liquid-phase-sintered silicon carbide during creep in an oxidizing environment. J Am Ceram Soc. 2003;86:501–7.
28. Stobierski L, Gubernat A. Sintering of silicon carbide II. Effect of boron. Ceram Int. 2003;29:355–61.
29. Petrus M, Wozniak J, Cygan T, Kostecki M, Olszyna A. The effect of the morphology of carbon used as a sintering aid on the mechanical properties of silicon carbide. Ceram Int. 2019;45:1820–4.
30. Petrus M, Wozniak J, Cygan T, Adamczyk-Cieslak B, Kostecki M, Olszyna A. Sintering behaviour of silicon carbide matrix composites reinforced with multilayer graphene. Ceram Int. 2017;43:5007–13.
31. Petrus M, Wozniak J, Jastrz A, Kostecki M, Cygan T, Olszyna A. The effect of the morphology of carbon used as a sintering aid on the sinterability of silicon carbide. Ceram Int. 2018;44:7020–5.
32. Lago DC, Prado MO. Crystallization of yttrium and samarium aluminosilicate glasses. Phys Procedia. 2013;48:10–6.
33. Kissinger HE. Reaction kinetics in differential thermal analysis. Anal Chem. 1957;29:1702–6.
34. Mittemeijer EJ. Review – analysis of the kinetics of phase transformations. J Mater Sci. 1992;27:3977–87.
35. Biesuz M, Spiridigliozzi L, Marocco A, Dell'Agli G, Sglavo VM, Pansini M. Sintering behavior of Ba/Sr celsian precursor obtained from zeolite-A by ion-exchange method. J Am Ceram Soc. 2017;100:5433–43.

How to cite this article: Popolizio A, Biesuz M, Molinari A, Sglavo VM. Spark plasma sintering of alumina/yttria-doped silicon carbide. *Int J Ceramic Eng Sci*. 2020;2:92–100. https://doi.org/10.1002/ces2.10038